CALCULATION OF THE PASSIVE AND ACTIVE COMPONENT STRESS OF THREE PHASE PWM CONVERTER SYSTEMS WITH HIGH PULSE RATE

Johann W. Kolar, Hans Ertl, Franz C. Zach, Technical University Vienna, Power Electronics Section
Gußhausstraße 27, Vienna, Austria

Aachen 1989

ABSTRACT

This paper treats the simplified purely analytical estimation of the stress of passive and active components of PWM converter systems. The approximation of the actual system behavior thereby is gained according to the generation of limit values or mean values, respectively. This is done by transition from a summation of the "local" contributions of the single pulse periods (related to the interval center) to the integration of a quasicontinuous time function of equal local power loss. The latter function is gained via shifting the pulse interval through the period given by the (voltage or current) fundamental period. A modification of the phase modulation functions allows furthermore the minimization of the harmonic losses on the AC side. (This minimization is immediately clear after transformation of the system variables into space vectors.) When compared to harmonic optimal modulation methods known so far the optimization given here results in considerably lower current harmonics rms values in the upper modulation region. Therefore it is especially well applicable to the control of PWM rectifier systems. As the comparison of the approximate solutions and of the results of a digital simulation shows, already for relatively low converter switching frequencies (low compared to the output frequency) a good consistency of the results is given. Therefore, the relationships derived can be applied immediately for the dimensioning of converter systems using FETs, BTs or IGBTs.

KEYWORDS

PWM Converter, Conduction Losses, Switching Losses, DC Link Capacitor Current, Optimization of Pulse Width Modulation

Introduction

PWM converter systems with voltage DC-link have found broad acceptance in industrial applications within the last years. In first line we have the use as converter for machines and drives (pulse width modulated (PWM) inverters), mains converters (PWM rectifiers), static VAR compensators etc. The common basis of the system mentioned is given by the basically equal circuit configuration of the power circuit (see Fig.1). The dimensioning of its active and passive components in any case is linked to a digital simulation or measurements of laboratory hardware models. This is also documented by the relatively high number of relevant publications in this problem area. A basic disadvantage of this method is, however, that any single simulation run can only give results for a single set of parameters (for a single point in the parameter space). In order to characterize the system behavior in the entire operating region one has to perform a multitude of simulation runs. Their results offer (if represented graphically in normalized form) only limited insight regarding the parameter dependency of the characteristic values. This is because only numeric values are gained by a simulation.

Starting from this situation which is not very satisfying from an engineering point of view (where an easy estimation of results would be desirable) this paper tries to do the following: for pulse converter systems with high pulse frequencies simple analytical relationships concerning the dependencies of the device stress on the operating parameters (DC link voltage, size of electric and magnetic storage elements, pulse frequency) shall be given.

The basics for this approach is given by an averaging method described in the following. It transfers discontinuous current and voltage forms into continuous signals which are approximately equal to with respect to the power losses. The comparison with the results of a digital simulation shows an excellent consistency for pulse frequencies which are high compared to the output frequency. Considering the high pulse frequencies realizeable with today's turn-off power semiconductor devices (BT, IGBT, FET, GTO), the insight into the stationary working behavior of modern PWM converter systems is essentially deepened. Furthermore, the equations given in this paper at the end of each section can be applied immediately as dimensioning basis.

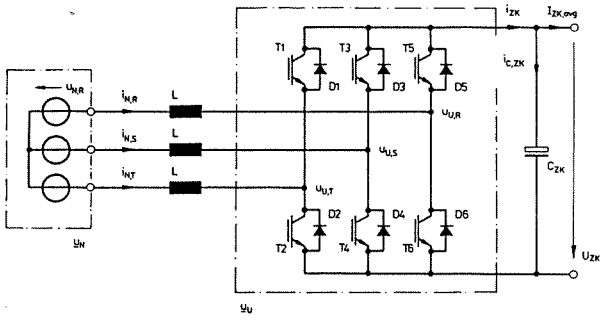

Fig.1: Structure of the power circuit of a three phase voltage DC link PWM converter system. For usage as *PWM inverter* for AC machine drives the inductances L and the three phase system $\underline{u}_N$ can be interpreted as simple equivalent circuit of the AC machine formed by leakage inductances and machine counter emf. On the other hand, for mains operation of the *converter* (PWM rectifier, static VAR compensator) the inductances have to be connected in series; the voltage system $\underline{u}_N$ is defined by the mains conditions.

Computation of the Conduction Losses

Due to the three phase structure of the system (identical structure of the phase legs) the analysis can be limited to the analysis of one phase leg (Fig.2). For the mean value related to one pulse interval (*local* mean value) of the converter voltage we have according to Fig.3:

$$\bar{u}_U(kT_P) = \frac{U_{ZK}}{2}[2\alpha(kT_P) - 1] \,. \qquad (1)$$

The running variable k giving the position of the pulse interval within the period given by the fundamental frequency has the range of values

$$k \in [0, (pz - 1)] \,. \qquad (2)$$

For the definition of the pulse number pz we have:

$$pz = \frac{f_P}{f_N} = \frac{T_N}{T_P} \; . \tag{3}$$

Assuming a sinusoidal output voltage (fundamental frequency) Eq. (1) yields

$$\bar{u}_U(\tau) = \hat{U}_U \sin \omega_N \tau \; . \tag{4}$$

Considering the definition of the modulation depth M we receive for the duty ratio α for the bridge leg (which in its basic function can be represented by a reversing switch)

$$\alpha(\tau) = \frac{1}{2}[1 + M \sin \omega_N \tau] \; , \tag{5}$$

$$M = \frac{2\hat{u}_U}{U_{ZK}} \; . \tag{6}$$

The variable τ thereby is set for identification of a *"macroscopic"* quasi-continuous behavior which is gained from the real signal

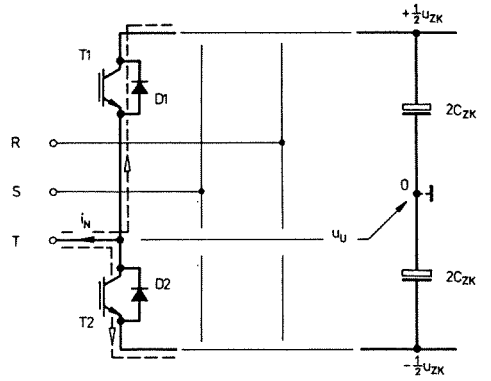

Fig.2: Division of the output current flowing into controlled and uncontrolled semiconductor devices of a PWM converter bridge leg

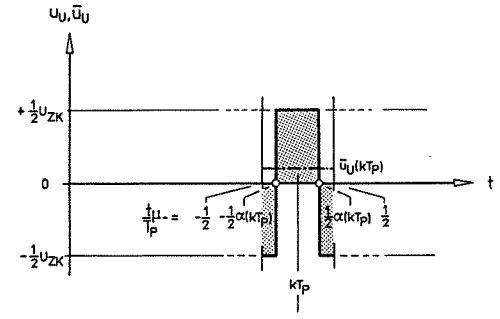

Fig.3: Formation of the converter output ("microscopic") mean value related to the pulse period; thereby a defined ("macroscopic") duty ratio is assumed

shape by averaging over a pulse period (the *"microscopic"* behavior). The resulting *"microscopic"* mean value always has to be related to the position of the pulse period which has to be considered as being moveable over the fundamental period. For higher pulse rates the mean value converges towards the converter output voltage fundamental.

According to Eq. (7) the conduction power losses of a bridge leg transistor have to be computed via the mean value of the product of the forward voltage drop and the collector current relative to the fundamental period.

$$P_{F,Ti} = \frac{1}{T_N} \int_{T_N} u_{F,Ti} i_{Ti} \, dt \tag{7}$$

If the forward characteristic of the semiconductor is approximated according to (see also Fig. 3)

$$u_{F,Ti} = U_{F,T} + r_{F,T} i_{Ti} \; , \tag{8}$$

we receive with

$$I_{Ti,avg} = \frac{1}{T_N} \int_{T_N} i_{Ti} \, dt \; , \tag{9}$$

$$I^2_{Ti,rms} = \frac{1}{T_N} \int_{T_N} i^2_{Ti} \, dt \; , \tag{10}$$

$$P_{F,Ti} = U_{F,T} I_{Ti,avg} + r_{F,T} I^2_{Ti,rms} \; . \tag{11}$$

The conduction losses are determined accordingly as well by the *mean value* as by the *rms value (by the form factor)* of the transistor current in general.

Similary we have for the non-controllable elements (diodes):

$$u_{F,Di} = U_{F,D} + r_{F,D} i_{Di} \tag{12}$$

$$P_{F,Di} = U_{F,D} I_{Di,avg} + r_{F,D} I^2_{Di,rms} \tag{13}$$

With respect to a mathematically simple formulation we make the following assumptions (for further considerations):

- Symmetric regular sampling
- Limitation to discrete phase angle values $\varphi_{\underline{u}_U, \underline{i}_N}$ such that the current zero crossings coincide always with the begin or the end of a pulse interval, respectively.
- $pz = 2i \qquad i = 1, 2, 3, \ldots$

As the further derivation shows, these assumptions do not limit the general validity of the results (i.e., for the derivation of the limit values). Evaluation of Eq.(9) leads to

$$\begin{aligned} p_{F,T1} \; &= \; U_{F,T} \left\{ \frac{1}{T_N} \sum_{k=0}^{k=(\frac{pz}{2}-1)} \int_{t_k - \alpha_k \frac{T_P}{2}}^{t_k + \alpha_k \frac{T_P}{2}} i_{Ti} \, dt \right\} + \\ &+ \; r_{F,T} \left\{ \frac{1}{T_N} \sum_{k=0}^{k=(\frac{pz}{2}-1)} \int_{t_k - \alpha_k \frac{T_P}{2}}^{t_k + \alpha_k \frac{T_P}{2}} i^2_{Ti} \, dt \right\} \; , \end{aligned} \tag{14}$$

with

$$t_k = \left[\frac{-\varphi}{\omega_N} + \frac{T_P}{2}(1 + 2k) \right] \; , \tag{15}$$

$$\varphi = \varphi_{\underline{u}_U, \underline{i}_N} \; , \tag{16}$$

$$\alpha_k = \alpha(t_k) \; . \tag{17}$$

According to Eq.(19) now the local integrations (point of time t_k) in Eq. (15) can be extended to the formulation of *microscopic mean values.*

$$\begin{aligned} P_{F,T1} = \; & U_{F,T} \; \left\{ \frac{1}{T_N} \sum \left[\frac{1}{T_P} \int i_{Ti} \, dt \right] T_P \right\} + \\ + \; & r_{F,T} \; \left\{ \frac{1}{T_N} \sum \left[\frac{1}{T_P} \int i^2_{Ti} \, dt \right] T_P \right\} \end{aligned} \tag{18}$$

For assuming infinitely high pulse frequency

$$T_P \; \rightarrow \; d\tau \tag{19}$$

$$\frac{\varphi}{\omega_N} + \frac{T_P}{2}(1 + 2k) \rightarrow \; \tau \tag{20}$$

(thereby the *microscopic* time *interval* T_P is converted into a *macroscopic* time *differential* or, the *discrete* points of time t_k are converted into the *continuous* time τ) we receive

$$i_{T1,avg}(\tau) = \frac{1}{T_P} \int_{-\alpha(\tau)\frac{T_P}{2}}^{\alpha(\tau)\frac{T_P}{2}} i_{T1}(\tau) \, dt_\mu = \alpha(\tau) i_{T1}(\tau) \; , \tag{21}$$

$$i^2_{T1,rms}(\tau) = \frac{1}{T_P} \int_{-\alpha(\tau)\frac{T_P}{2}}^{\alpha(\tau)\frac{T_P}{2}} i^2_{T1}(\tau) \, dt_\mu = \alpha(\tau) i^2_{T1}(\tau) \; . \tag{22}$$

A timewise discontinuous signal therefore is converted into one with equal power loss (equal linear and quadratic current mean values; see Fig.4). The result of the local averaging on one hand can be interpreted as evaluation of a (macroscopic) infinitely small pulse interval; on the other hand, it can be interpreted

as the calculation of a mean value over a (macroscopic) finitely wide interval, being related to the interval center. For a finitely wide pulse interval thereby an only linear approximation of the current shape to be integrated is assumed. The evaluation of the macroscopic mean values (relative to the fundamental) which is really interesting for calculation of the conduction losses can be

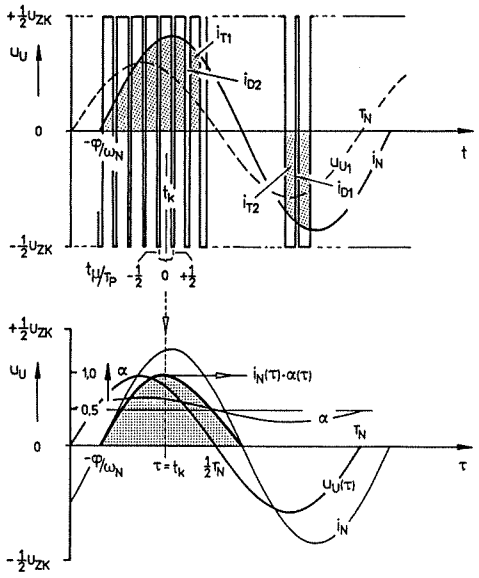

performed via Eqs.(21,22) in a simple manner in closed form by

$$P_{F;T1} = U_{F,T}\left\{\frac{1}{T_N}\int_{\frac{-\varphi}{\omega_N}}^{\frac{-\varphi+\pi}{\omega_N}} i_{T1,avg}(\tau)\,d\tau\right\} + + r_{F,T}\left\{\frac{1}{T_N}\int_{\frac{-\varphi}{\omega_N}}^{\frac{-\varphi+\pi}{\omega_N}} i^2_{T1,rms}(\tau)\,d\tau\right\} . \quad (23)$$

Based on a purely sinusiodal output current with general phase angle with respect to the converter output voltage

$$i_N(t) = \hat{I}_N \sin(\omega_N t + \varphi) . \quad (24)$$

the averaging method shall be briefly analyzed in the following. It is sensible to compare the local contribution of the exact calculation

$$s_{t_k} = \int_{t_k-\alpha_k\frac{T_P}{2}}^{t_k+\alpha_k\frac{T_P}{2}} i_{Ti}\,dt , \quad (25)$$

to the expression gained by application of the averaging method

$$\bar{s}_{t_k} = \int_{t_k-\frac{T_P}{2}}^{t_k+\frac{T_P}{2}} i_{Ti}(\tau)\alpha(\tau)\,d\tau . \quad (26)$$

A brief calculation (not given here) shows that the deviation of the approximate solution only appears for a higher than first power of the pulse period (normalized with respect to the fundamental period). This very good consistency is also given for the macroscopic mean value as shown in Figs.5 and 6 based on a relative error definition given by

$$f_{I;Ti,avg} = \frac{\left[\int_{-\varphi/\omega_N}^{(-\varphi+\pi)/\omega_N} i_{Ti,avg}(\tau)\,d\tau - \sum_k \int_{T_P(k)} i_{Ti}\,dt\right]}{\sum_k \int_{T_P(k)} i_{Ti}\,dt} . \quad (27)$$

As Fig.6 shows, the amount of the deviation is essentially determined by the amount of the modulation and by the phase shift between modulating function and output current. For the sake of brevity we want to omit here a closer discussion of the error (amount) area which can be interpreted easily.

The statements made so far for the macroscopic linear mean value are also confirmed for the macroscopic quadratic mean value. This is according to Fig.7 based on an analogous error definition

$$s'_{t_k} = \int_{t_k-\alpha_k\frac{T_P}{2}}^{t_k+\alpha_k\frac{T_P}{2}} i^2_{Ti}\,dt , \quad (28)$$

$$\bar{s}'_{t_k} = \int_{t_k-\frac{T_P}{2}}^{t_k+\frac{T_P}{2}} i^2_{Ti}(\tau)\alpha(\tau)\,d\tau , \quad (29)$$

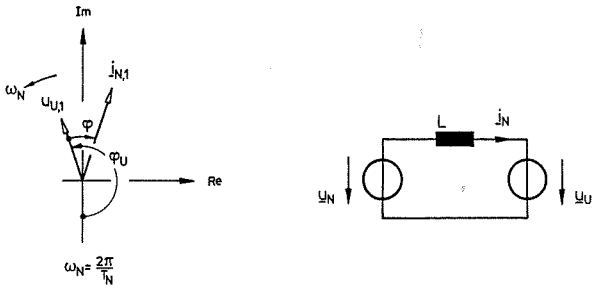

Fig.4: Application of the averaging method for calculation of a continuous time function corresponding to the local ("microscopic") mean value of i_{T1}

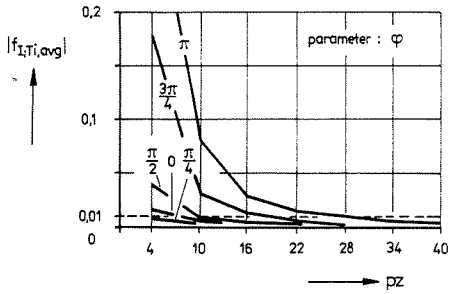

Fig.5: Value of the relative error of the analytically closed approximation of the linear ("macroscopic") transistor current mean value

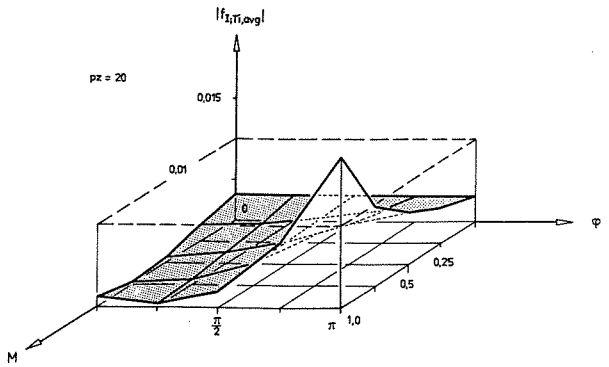

Fig.6: Relative error of the approximation method (linear averaging method) in dependency on the modulation depth and the phase angle

$$f_{I^2;Ti,rms} = \frac{\left[\int_{-\varphi/\omega_N}^{(-\varphi+\pi)/\omega_N} i^2_{Ti,rms}(\tau)\,d\tau - \sum_k \int_{T_P(k)} i^2_{Ti}\,dt\right]}{\sum_k \int_{T_P(k)} i^2_{Ti}\,dt} . \quad (30)$$

Based on Eq.(23), the computation of the local conduction losses of the transistor T1 or the Diode D2, respectively, leads to

$$p_{F,T1}(\varphi_U) = \frac{U_{F,T}\hat{I}_N}{2}[1 + M\sin\varphi_U]\left[1 + \frac{r_{F,T}\hat{I}_N}{U_{F,T}}\sin(\varphi_U+\varphi)\right] \cdot \sin(\varphi_U+\varphi)\ , \quad (31)$$

$$p_{F,D2}(\varphi_U) = \frac{U_{F,D}\hat{I}_N}{2}[1 - M\sin\varphi_U]\left[1 + \frac{r_{F,D}\hat{I}_N}{U_{F,D}}\sin(\varphi_U+\varphi)\right] \cdot \sin(\varphi_U+\varphi)\ . \quad (32)$$

Thereby the validity of these equations is limited to the interval

$$\varphi_U = \omega_N\tau \qquad \varphi_U \in [-\varphi, -\varphi+\pi]\ , \quad (33)$$

dependent on the output current direction and on the phase angle counting direction (determined in Fig.4). The macroscopic power loss behavior determined herewith will form an essential base for dimensioning the semiconducters especially for low output frequency. This is because then there is no sufficient averaging (for defined thermal time constant) resulting in largely constant junction temperature. For higher output frequencies (or for corresponding thermal inertia) the relationships

$$\boxed{P_{F,T1} = \frac{U_{F,T}\hat{I}_N}{2}\left[\frac{1}{\pi} + \frac{M}{4}\cos\varphi\right] + r_{F,T}\hat{I}_N^2\left[\frac{1}{8} + \frac{M}{3\pi}\cos\varphi\right]\ ,} \quad (34)$$

$$\boxed{P_{F,D2} = \frac{U_{F,D}\hat{I}_N}{2}\left[\frac{1}{\pi} - \frac{M}{4}\cos\varphi\right] + r_{F,D}\hat{I}_N^2\left[\frac{1}{8} - \frac{M}{3\pi}\cos\varphi\right]\ ,} \quad (35)$$

can be used. The sum of the conduction losses of one half of a bridge leg will be (based on Eqs.(34,35)) determined by

$$P_F = 2(P_{F,T1} + P_{F,D2})\ , \quad (36)$$

$$\boxed{\begin{aligned} P_F &= \tfrac{\hat{I}_N}{\pi}(U_{F,T}+U_{F,D}) + \tfrac{M\hat{I}_N}{4}(U_{F,T}-U_{F,D})\cos\varphi + \\ &+ \tfrac{\hat{I}_N^2}{4}(r_{F,T}+r_{F,D}) + \tfrac{2M\hat{I}_N^2}{3\pi}(r_{F,T}-r_{F,D})\cos\varphi\ . \end{aligned}} \quad (37)$$

If one assumes constant forward voltage drop (independent of the current magnitude) of the semiconductors, Eq.(37) can be simplified according to

$$\boxed{P_F \approx 0.5 U_F I_{N,rms}\ .} \quad (38)$$

Thereby one has to choose U_F as average value between transistor and diode forward voltage.

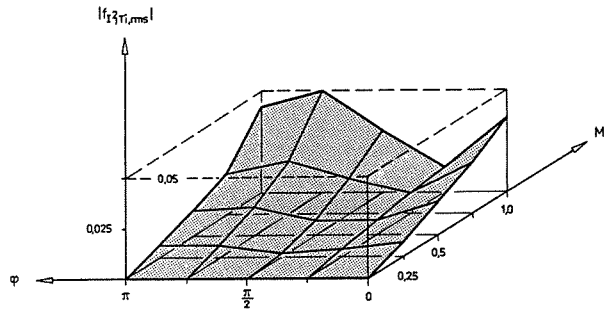

Fig.7: Relative error of the approximation method (generation of a quadratic macroscopic mean value) in dependency on the modulation depth and the phase angle

Similary to the calculation method for the conduction losses one can via

$$\beta_{T1} = \frac{1}{2\pi}\int_{-\varphi}^{-\varphi+\pi} 1.\alpha\ d(\omega_N\tau)\ , \quad (39)$$

$$\beta_{D2} = \frac{1}{2\pi}\int_{-\varphi}^{-\varphi+\pi} 1.(1-\alpha)\ d(\omega_N\tau) \quad (40)$$

easily give the average duty ratio of the diodes and transistores of the bridge leg (which is interesting from a theoretical point of view) by

$$\beta_T = \beta_{T1} + \beta_{T2} = 2\beta_{T1} = \frac{1}{2} + \frac{M}{\pi}\cos\varphi\ , \quad (41)$$

$$\beta_D = 1 - \beta_T = \frac{1}{2} - \frac{M}{\pi}\cos\varphi\ . \quad (42)$$

As Fig.8 shows, the conduction period of the semiconductors rises and falls with increasing modulation. With increasing $\cos\varphi$ it is shifted from the uncontrolled to the controlled semiconductor devices. $\cos\varphi = +1$ in any case means power flow out of the DC link. Then, as given before, mainly the transistors conduct the current.

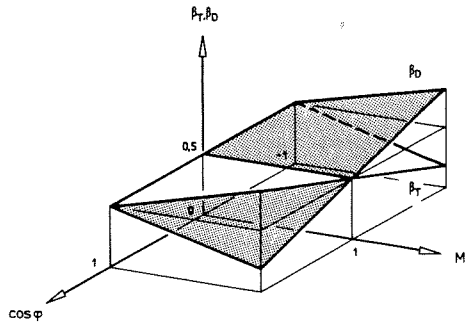

Fig.8: Relative conduction period of the controlled and uncontrolled semiconductor devices in dependency on the modulation depth and the phase angle

Calculation of the Switching Losses

Besides the determination of the conduction losses especially for higher switching frequencies the calculation of the switching losses of the semiconductor devices is important for thermal dimensioning of the power circuit. Thereby there exists basically a variety of thinkable approaches from which two are described briefly in the following.

If the switching losses are gained via parameters known from data sheets or from measurements of the switching behavior (fall time etc.) we have, e.g., for rough approximation of the local turn-off energy loss (L_σ — parasitic inductance of the circuit)

$$w_{off,T1} = \frac{1}{2}[i_{T1}^2 L_\sigma + i_{T1}U_{ZK}t_{f0,T} + i_{T1}^2 k_{f,T}U_{ZK}]\ . \quad (43)$$

Thereby a linear approximation of the current dependency of the fall time according to

$$t_{f,T} = t_{f0,T} + k_{f,T}i_T \qquad [k_{f,T}] = \frac{s}{A} \quad (44)$$

is assumed. With

$$p_{off}(\tau) = w_{off}\{i_T(\tau)\}f_P\ , \quad (45)$$

$$P_{off,T1} = \frac{1}{2\pi}\int_{-\varphi}^{-\varphi+\pi} p_{off,T1}(\omega_N\tau)d(\omega_N\tau) \quad (46)$$

we receive for the macroscopic turn-off power loss

$$P_{off,T1} = \left\{\frac{\hat{I}_N U_{ZK}}{\pi}t_{f0,T} + \frac{\hat{I}_N^2}{4}[L_\sigma + k_{f,T}U_{ZK}]\right\}f_P\ . \quad (47)$$

Giving a falltime for the actual current shape during the switching interval is very insufficient, especially when tail-currents are present; therefore it is much more meaningful to start with a measurement of the turn-off energy loss for a defined parameter set (DC link voltage, juction temperature, ...). The switching energy loss (turn-on and turn-off losses) appearing within a pulse

interval therefore can be given immediately for controlled and uncontrolled valves in dependency on the current being switched. Starting from Eq.(47) or from a measurement method for the shape of the characteristics (not described in detail here) a quadratic approximation

$$w_{P,T}\{i_T(\omega_N\tau)\} = k_{1,T}i_T + k_{2,T}i_T^2 \,, \tag{48}$$

$$[k_{1,T}] = \frac{Ws}{A} \quad [k_{2,T}] = \frac{Ws}{A^2} \tag{49}$$

is recommended. With

$$p_{P,T} = w_{P,T}f_P \tag{50}$$

$$P_{P,T1} = \frac{1}{2\pi}\int_{-\varphi}^{-\varphi+\pi} p_{P,T1}\{\omega_N\tau)\}\, d(\omega_N\tau) \tag{51}$$

it follows for the switching power loss of a transistor

$$\boxed{P_{P,T1} = \hat{I}_N\left(\frac{k_{1,T}}{\pi} + \hat{I}_N\frac{k_{2,T}}{4}\right)f_P} \tag{52}$$

wherefore an estimate can be given in a simple manner according to

$$\boxed{k_{2,T} = 0 \quad P_{P,T} \approx 0.5k_{1,T}I_{N,rms}f_P \,.} \tag{53}$$

One has to observe that Eq.(52) implies a linear dependency of the switching losses on the pulse frequency (independent, however, of the averaging method used here).

The total losses of a bridge leg transistor result (together with Eq.34) in

$$\boxed{\begin{aligned} P_{T1} &= \left\{\frac{U_{P,T}}{2}\left[\frac{1}{\pi}+\frac{M}{4}\cos\varphi\right] + \frac{k_{1,T}f_P}{\pi}\right\}\hat{I}_N + \\ &+ \left\{r_{P,T}\left[\frac{1}{8}+\frac{M}{3\pi}\cos\varphi\right] + \frac{k_{2,T}f_P}{4}\right\}\hat{I}_N^2 \,. \end{aligned}} \tag{54}$$

Eqs.(54) and (34) allow furthermore a comparison of the conduction and switching losses of a valve. Also, for given maximum allowable power loss (according to a maximum junction temperature) one can give (based on Eq.(54) the dependency of the allowable AC current peak value on modulation and $\cos\varphi$. This limit forms one of the border lines of the converter operating region.

For the uncontrolled valves basically analogous simple relationships are valid which could be based on the given considerations. The respective treatment shall be omitted here.

Calculation of the DC-Link-Current Parameters

Because the capacitance of an electrolytic-capacitor can be linked to a defined current carrying capability, the size of the DC link capacitor is essentially determined (among other things) by the capacitor current rms value.

For a symmetric three phase voltage (current) system

$$\begin{aligned} \alpha_R &= \frac{1}{2} + \frac{M}{2}\sin\omega_N t \\ \alpha_S &= \frac{1}{2} + \frac{M}{2}\sin\left(\omega_N t - \frac{2\pi}{3}\right) \\ \alpha_T &= \frac{1}{2} + \frac{M}{2}\sin\left(\omega_N t + \frac{2\pi}{3}\right) \,, \end{aligned} \tag{55}$$

$$\begin{aligned} i_{N,R} &= \hat{I}_N\sin\left(\omega_N t + \varphi\right) \\ i_{N,S} &= \hat{I}_N\sin\left(\omega_N t + \varphi - \frac{2\pi}{3}\right) \\ i_{N,T} &= \hat{I}_N\sin\left(\omega_N t + \varphi + \frac{2\pi}{3}\right) \end{aligned} \tag{56}$$

at the input of the PWM converter considered, segments of the ac side currents are switched into the DC link according to the switching status (see Fig.9). For the mean value or the rms value of the DC link current we have then in the interval

$$\varphi_U = \omega_N\tau \in \left[\left(\pi - \frac{\pi}{6}\right), \left(\pi + \frac{\pi}{6}\right)\right] \,, \tag{57}$$

$$\begin{aligned} i_{ZK,avg}(\tau) &= -i_{N,T}(\tau)\left[\alpha_R(\tau) - \alpha_T(\tau)\right] + \\ &+ i_{N,S}(\tau)\left[\alpha_S(\tau) - \alpha_R(\tau)\right] \,, \end{aligned} \tag{58}$$

$$\begin{aligned} i^2_{ZK,rms}(\tau) &= i^2_{N,T}(\tau)\left[\alpha_R(\tau) - \alpha_T(\tau)\right] + \\ &+ i^2_{N,S}(\tau)\left[\alpha_S(\tau) - \alpha_R(\tau)\right] \,. \end{aligned} \tag{59}$$

The local DC link current mean value due to the time constant power flow of a symmetric three phase system also shows a time independent value

$$\boxed{i_{ZK,avg}(\tau) = \frac{3}{4}\hat{I}_N m\cos\varphi = I_{ZK,avg} \,.} \tag{60}$$

For the macroscopic DC link current rms value

$$I^2_{ZK,rms} = \frac{3}{\pi}\int_{\left(\pi-\frac{\pi}{6}\right)}^{\left(\pi+\frac{\pi}{6}\right)} i^2_{ZK,rms}\{\omega_N\tau\}\, d(\omega_N\tau) \tag{61}$$

(due to the 60° periodicity of the DC link current shape averaging can be limited to a sixth of the base period) there follows

$$\boxed{I^2_{ZK,rms} = \frac{\sqrt{3}}{\pi}M\hat{I}_N^2\left(\frac{1}{4} + \cos^2\varphi\right) \,.} \tag{62}$$

For constant load of the DC link therefore the capacitor current rms value can be determined via

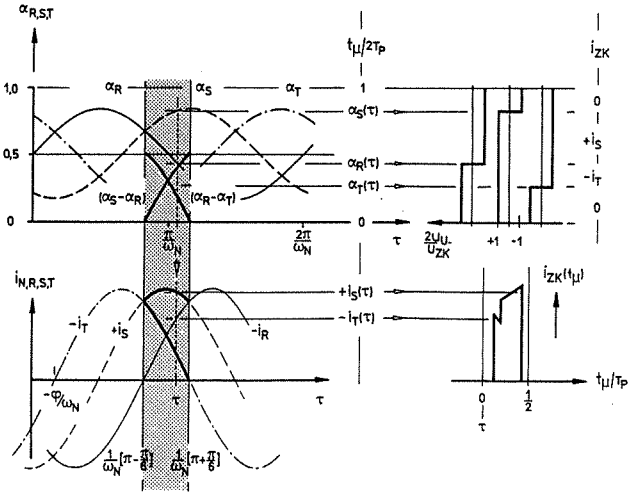

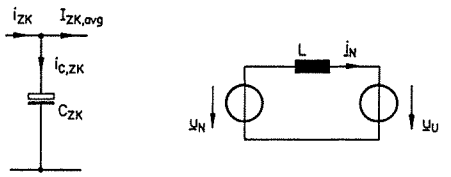

Fig.9: Switching status dependent generation of the DC link current via phase current segments

$$i_{ZK} = i_{C,ZK} + I_{ZK,avg} \ , \tag{63}$$

$$\int_{T_N} i_{C,ZK} I_{ZK,avg} d\tau \ = \ 0 \ , \tag{64}$$

$$I^2_{ZK,rms} = I^2_{C,ZK,rms} + I^2_{ZK,avg} \tag{65}$$

as

$$\boxed{I^2_{C,ZK,rms} = M\hat{I}^2_N \left[\frac{3}{4\pi} + \cos^2\varphi \left(\frac{\sqrt{3}}{\pi} - \frac{9}{16}M\right)\right]} \tag{66}$$

(see also Fig.10). For $\cos\varphi = 0$ for the then disappearing mean value of I_{ZK} the rms value $I_{C,ZK,rms}$ coincides with $I_{ZK,rms}$. The maximum of the shape of $I_{C,ZK,rms}$ at M ($\cos\varphi \approx +-1$) can be explained by the dependency of the DC link current mean value on the modulation M. Regarding a worst case consideration especially the evaluation of Eq.(66) is of importance for the value

$$M' = \frac{8\sqrt{3}}{9\pi}\left(1 + \frac{1}{4\cos^2\varphi}\right) \tag{67}$$

which is related to the maximum. Thereby with decreasing $\cos\varphi$ the maximum value mentioned before is turned into a boundary maximum (not given by Eq.(67)) occurring at $M = 1$ (for sinusoidal modulation) or at $M = 2/\sqrt{3}$ (achievable by a modification of the modulation approach).

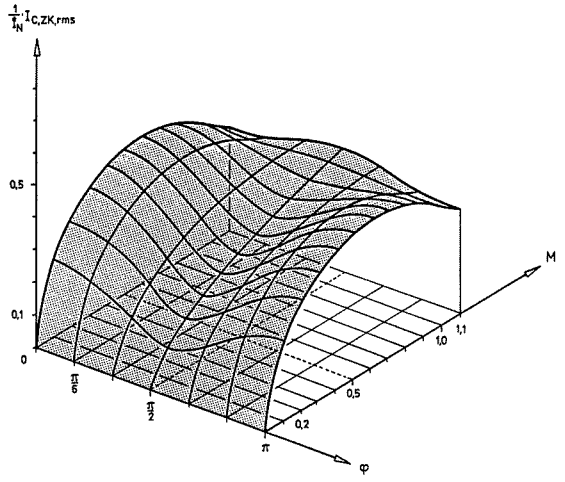

Fig.10: Dependency of the DC link capacitor current rms value on modulation depth and phase angle

As can be seen from Fig.11 for a characteristic parameter set, already for relatively low pulse frequency very good convergence is given for the DC link current values which are determined via Eqs.(62) and (66) (when compared to the values gained via digital simulation). Basically in Eqs.(62) and (66) there is no dependency on pulse frequency and value of the inductances on the AC side (which also can be leakage inductances of an AC machine); this is according to the assumption of purely sinusoidal currents (or neglection of harmonics). Therefore, generally for a sufficiently smooth phase current shape one can assume a good approximation of exact results by the equations given.

Calculation of the AC Side Harmonic Losses

Besides application of the averaging method described for calculation of characteristic values as a basis for dimensioning the power semiconductors (as well as for the DC side energy storage, i.e. the DC link capacitor) the averaging method can also be used for determination of the AC side harmonic losses. This topic will be treated in detail in a future paper now being in preparation. Here, for the sake of completeness, essential results shall be presented.

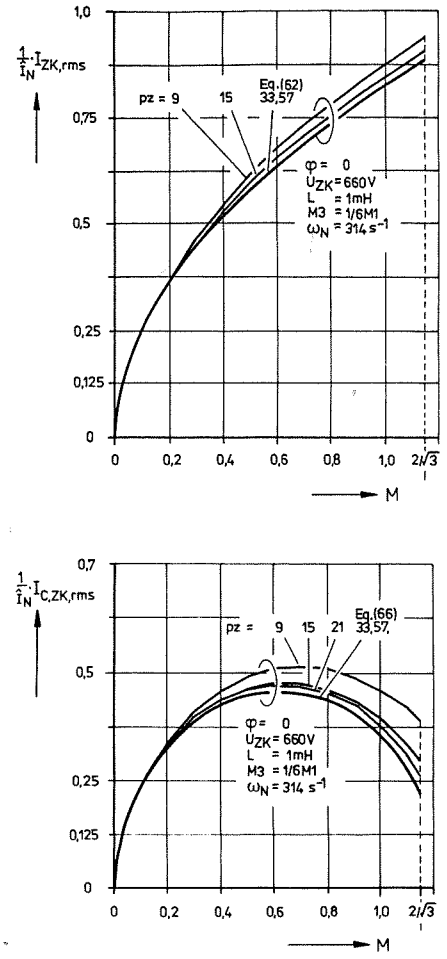

Fig.11: Comparison of the results of the approximation method and the digital simulation

With

$$\Delta i_n = \frac{U_{ZK}}{4}\frac{T_P}{2L} \ , \tag{68}$$

$$\varphi'_U = \omega_N \tau' = \varphi_U - \frac{\pi}{2} \ , \tag{69}$$

$$m(\tau') = \frac{2u_U(\tau')}{U_{ZK}} = [2\alpha(\tau') - 1] \tag{70}$$

there follows for the rms value of the current harmonics for sinusoidal modulation — designated by subscript [1]

$$\boxed{\Delta I^2_{N,rms,[1]} = \frac{1}{6}\Delta i^2_n M^2 \left[1 - \frac{8M}{\sqrt{3}\pi} + \frac{3M^2}{4}\right]} \ . \tag{71}$$

Thereby the modulation is limited to $M \leq 1$, however.

If one applies a modulation method (which in general is called *space vector modulation)* — designateded by subscript [2], one can increase the modulation range up to the theoretical limit ($M_{max} = 2/\sqrt{3}$) which is achievable without overmodulation. Furthermore the harmonic losses can be reduced considerably according to

$$\boxed{\Delta I^2_{N,rms,[2]} = \frac{1}{6}\Delta i^2_n M^2 \left[1 - \frac{8M}{\sqrt{3}\pi} + \frac{9M^2}{8}\left(1 - \frac{3\sqrt{3}}{4\pi}\right)\right]} \tag{72}$$

if compared to sinusoidal modulation (see Fig.16). For the related modulation functions (Fig.12) we have

$$[2]: \ M \leq \frac{2}{\sqrt{3}}; \ \varphi'_U \in \left[\frac{\pi}{3}, \frac{2\pi}{3}\right]: \ m_R = \frac{3}{2}M\cos\varphi'_U$$

$$m_S = \frac{\sqrt{3}M}{2}\sin\varphi'_U$$

$$m_T = -\frac{\sqrt{3}M}{2}\sin\varphi'_U \tag{73}$$

The shape of the modulation functions in the entire base interval thereby can easily be determined by cyclic extension corresponding to the phase axis sequence for rotation of the converter voltage space vector to be produced.

A closer analysis of the current harmonics space vector trajectory shows that the only available degree of freedom for a pulse pattern optimization in general lies in selecting the distribution of the free-wheeling states within a pulse half period. The modulation function shape (which results in an optimal behavior of the harmonics) can be gained immediately from the knowledge of the analytic dependency of the harmonic losses on the distribution mentioned before. Thereby one can approximate very well the shape of this optimal modulation functions by functions given by Eq.(73).

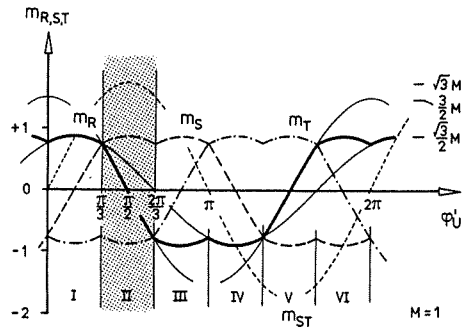

Fig.12: Shape of the phase modulation function according to Eq.(73) or [2], respectively

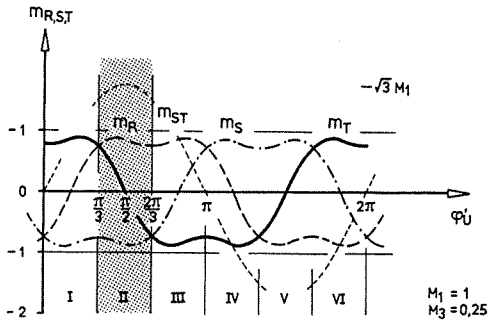

Fig.13: Shape of the phase modulation function according to Eq.(75) or [3], respectively

According to

$$\boxed{\Delta I^2_{N,rms,[3]} = \tfrac{1}{6}\Delta i_n^2 M_1^2 \left\{ 1 - \tfrac{8M_1}{\sqrt{3}\pi} + \right.} \\ \boxed{\left. + \tfrac{3M_1^2}{4}\left[1 - \tfrac{M_3}{M_1}\left(1 - 2\tfrac{M_3}{M_1}\right)\right]\right\}} \qquad (74)$$

also for "correction" of the simple sinusoidal modulation by addition of a third harmonic (Fig.13) with appropriate amplitude a harmonic loss minimization is possible (Fig.16). For definition of the modulation depth we have

$$M_1 = \frac{2u_{U,1}}{U_{ZK}}\,, \qquad M_3 = \frac{2u_{U,3}}{U_{ZK}}\,. \qquad (75)$$

The modulation functions follow as

$$\begin{aligned} m_R &= M_1 \cos\varphi'_U + \frac{M_3}{2}\cos 3\varphi'_U\,, \\ m_S &= M_1 \cos\left(\varphi'_U - \frac{2\pi}{3}\right) - \frac{M_3}{2}\cos 3\varphi'_U\,, \\ m_T &= M_1 \cos\left(\varphi'_U + \frac{2\pi}{3}\right) - \frac{M_3}{2}\cos 3\varphi'_U\,. \end{aligned} \qquad (76)$$

A minor disadvantage of the optimization

$$\left.\frac{M_3}{M_1}\right|_{J=min} = \frac{1}{4} \qquad (77)$$

is given, however, by a minor limitation of the overmodulation-free modulation range

$$\left.M_{1,max}\right|_{\frac{M_3}{M_1}=\frac{1}{4}} = 0.972\,\frac{2}{\sqrt{3}}\,. \qquad (78)$$

The entire modulation range can be used only in the suboptimal point

$$\left.\frac{M_3}{M_1}\right|_{J\approx min} = \frac{1}{6}\,. \qquad (79)$$

Common to all modulation methods treated so far is the generation of *phase* voltages which are sinusoidal in the average; they can be possibly also be "corrected" by harmonic of the order 3 and multiples of 3. The reference point is the (ficticious) center point of the DC link voltage. The voltages act on the outside only according to their differences forming the line to line voltages. So called zero components therefore are not projected into the output variables (this also can be shown immediately by space vector calculus; furthermore a three-wire system (neutral not connected) is assumed).

Alternatively one can choose not only the DC link center point as reference point of the resulting phase voltage system, but also (alternating) the positive and negative DC link rail. Furthermore, one can (in cyclic sequence) assume the switching status of always one converter phase according to the modulation functions (Figs.14,15)

$$\begin{aligned} [4]:\ M \le \frac{2}{\sqrt{3}}\ \varphi'_U \in \left[\frac{\pi}{3},\frac{\pi}{2}\right]:\ m_R &= 1 - \sqrt{3}M\sin\left(\varphi'_U - \frac{\pi}{3}\right) \\ m_S &= +1 \\ m_T &= 1 - \sqrt{3}M\sin\varphi'_U \\ \varphi'_U \in \left[\frac{\pi}{2},\frac{2\pi}{3}\right]:\ m_R &= \sqrt{3}M\sin\left(\varphi'_U + \frac{\pi}{3}\right) - 1 \\ m_S &= \sqrt{3}M\sin\varphi'_U - 1 \\ m_T &= -1\,, \end{aligned} \qquad (80)$$

$$\begin{aligned} [5]:\ M \le \frac{2}{\sqrt{3}}\ \varphi'_U \in \left[\frac{\pi}{3},\frac{\pi}{2}\right]:\ m_R &= \sqrt{3}M\sin\left(\varphi'_U + \frac{\pi}{3}\right) - 1 \\ m_S &= \sqrt{3}M\sin\varphi'_U - 1 \\ m_T &= -1 \\ \varphi'_U \in \left[\frac{\pi}{2},\frac{2\pi}{3}\right]:\ m_R &= 1 - \sqrt{3}M\sin\left(\varphi'_U - \frac{\pi}{3}\right) \\ m_S &= +1 \\ m_T &= 1 - \sqrt{3}M\sin\varphi'_U \end{aligned} \qquad (81)$$

as being fixed within an time interval. The two remaining coverter phases then have to be controlled by pulse width modulation such

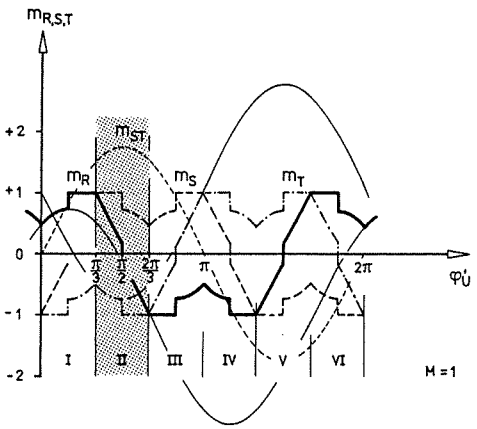

Fig.14: Shape of the phase modulation function according to Eq.(80) or [4], respectively

that the line to line voltages (gained by referencing these two phase voltages to the third) yield sinusoidal forms as a "pulse interval average".

By application of this approach one can increase the converter pulse frequency by a factor of 3/2 as compared to methods used so far. This can be seen immediately from the shape of the modulation functions; the average converter switching frequency remains the same. Thereby one can also shift the audible noise producing frequencies into higher regions. A further advantage becomes clear when one determines the resulting harmonic rms values

$$\Delta I^2_{N,rms,[4]} = \tfrac{1}{6}\Delta i_n^2 M^2 \left[4 - \tfrac{M}{\sqrt{3}\pi}\left(62 - 15\sqrt{3}\right) + \right. \\ \left. + \tfrac{9M^2}{8}\left(2 + \tfrac{\sqrt{3}}{\pi}\right)\right], \qquad (82)$$

$$\Delta I^2_{N,rms,[5]} = \tfrac{1}{6}\Delta i_n^2 M^2 \left[4 - \tfrac{M}{\sqrt{3}\pi}\left(8 + 15\sqrt{3}\right) + \right. \\ \left. + \tfrac{9M^2}{8}\left(2 + \tfrac{\sqrt{3}}{\pi}\right)\right]. \qquad (83)$$

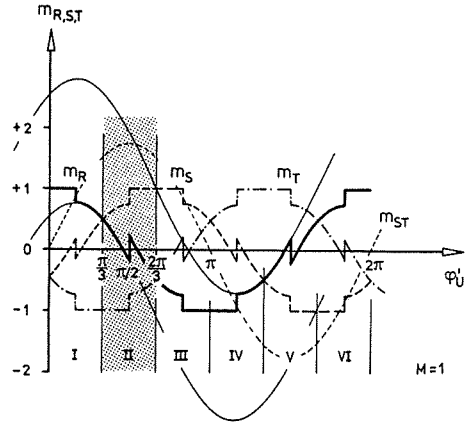

Fig.15: Shape of the phase modulation function according to Eq.(81) or [5], respectively

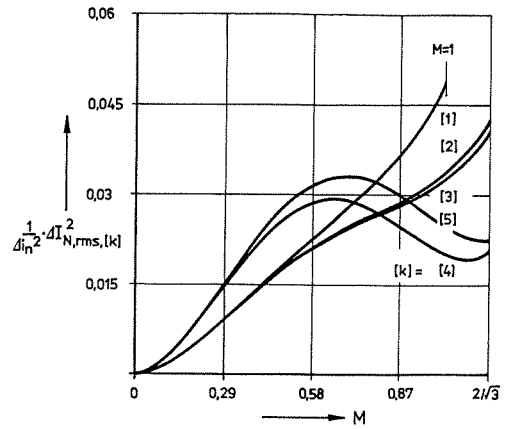

Fig.16: Comparison of the normalized harmonic power losses for various modulation methods

These lie (see Fig.16) when related to the same average converter switching frequency in the upper modulation region about 50% below the values of the modulation methods mentioned in the beginning of this paper (methods which have been described as harmonic optimal so far). Especially for PWM rectifier systems the new modulation method proposed here seems to be optimally suited because these systems always operate close to a modulation depth of 1 in the stationary case according to the approximately constant mains voltage.

Conclusions

As this paper shows the introduction of a simple averaging method makes possible the calculation of closed form analytical relationships which characterize the component stress of PWM converters with high pulse frequency. Furthermore this approach can be used for evaluation of the quality function of the optimization of a control method. In general, there exists the possibility to analyze and approximate a multitude of problems arising in connection with the operation of three phase (and also for single phase) PWM converter systems (e.g., current dependent distortion of the converter output voltage due to the forward voltage drop of the power semiconductor devices, or due to switching time delays).

In this connection one has to point out in principle that thereby (for calculation in three-wire systems) the application of space vector calculus offers essential advantages concerning transparency and possibilities of interpretation and extension of results when compared to using phase variables.

References

In the following a short collection of publications of special importance for this paper is given. There is no claim of completeness made. Due to the partial comparability of the results or a similar derivation method used the papers of VAN DER BROEK, SKUDELNY and STANKE, IKEDA, ITSUMI and FUNATO and SCHÖNUNG and BRENNEISEN have to be especially mentioned.

Boys, J. T. (1988) *Novel Current Sensor for PWM AC Drives.* IEE Proceedings, Vol. 135, Pt.B, No. 1, 27–32.

van der Broeck, H. W., Skudelny, H. C. and Stanke, G. V. (1988) *Analysis and Realization of a Pulsewidth Modulator Based on Voltage Space Vectors.* IEEE Transactions on Industry Application, Vol. IA-24, No.1, 142–150.

Ikeda, Y., Itsumi, J. and Funato, H. (1988) *The Power Loss of the PWM Voltage-Fed Inverter.* PESC '88 Record (April 1988), 277–283.

Mestha, L. K. and Evans, P. D. (1988) *Optimization of Losses in PWM Inverters.* IEE Conference Publication, No. 291, 394–397.

Nishizawa, J., Tamamushi, T. and Nonaka, K. (1987) *The Experimental and Theoretical Study on the High Frequency and High Efficiency SI Thyristor Type Sinusoidal PWM Inverter.* Proceedings of the 14th PCI '87 Conference, 167–181.

Rockot, J. H. (1987) *Losses in High-Power Bipolar Transistors.* IEEE Transactions on Power Electronics, Vol. PE-2, No. 1, 72–80.

Rosa, J. (1982) *The Harmonic Spectrum of DC Link Currents in Inverters.* Proceedings of the 4th PCI '82 Conference, 38–52.

Schönung, A. and Brenneisen, J. (1969) *Bestimmungsgrößen des selbstgeführten Stromrichters in sperrspannungsfreier Schaltung bei Steuerung nach dem Unterschwingungsverfahren.* ETZ-A, Bd. 90, H. 14, 353–357.

Sneyers, B., Lataire, Ph., Maggetto, G., Detemmerman, B. and Bodson, J. M. (1987) *Improved Voltage Source GTO Inverter with New Snubber Design.* European Power Electronic Conference, Vol. 1, 31–36.

Taufiq, J. A., Goodman, C. J. and Mellitt, B. (1986) *Railway Signalling Compatibility of Inverter Fed Induction Motor Drives for Rapid Transit.* IEE Proceedings, Vol. 133, Pt. B, No. 2, 71– 84.

Ziogas, P. D. and Photiadis, P. (1982) *An Exact Input Current Analysis of Ideal Static PWM Inverters.* IEEE Proceedings of IAS-82, 813–822.

Ziogas, P. D., Wiechmann, E. P. and Stefanovic, V. R. (1985) *A Computer-Aided Analysis and Design Approach for Static Voltage Source Inverters.* IEEE Transactions on Industry Applications, Vol. IA-21, No. 5, 1234–1241.

ACKNOWLEDGEMENT

The authors are very much indebted to the Austrian FONDS ZUR FÖRDERUNG DER WISSENSCHAFTLICHEN FORSCHUNG who supports the work of the Power Electronics Section at their university.